REPRODUCIBILITY OF COMPLEX TURBULENCE FLOW USING COMERCIALLY AVAIALBE CFD SOFTWARE

—FOR THE CASE OF A THREE-DIMENSIONAL ISOLATED-HILL WITH STEEP SLOPES—

Takanori UCHIDA and Graham Li

E-mail of corresponding author: *takanori@riam.kyushu-u.ac.jp*

Abstract

Selecting a high-quality site for wind turbine installation is frequently challenging in Japan because the majority of the topography of Japan is steep complex terrain and the spatial distribution of the wind speed is quite complex over such terrain. To address this issue, an unsteady CFD model called RIAM-COMPACT® has been developed. RIAM-COMPACT® is based on an LES turbulence model. In the present paper, to assess the accuracy of RIAM-COMPACT®, we performed a numerical simulation of uniform, non-stratified airflow past a three-dimensional isolated hill. Attention is focused on airflow characteristics in the wake region. The results of RIAM-COMPACT® using the LES model were in good agreement with those of another commercially available CFD software (STAR-CCM+) using LES models.

Key words: *CFD, Commercially available CFD software, STAR-CCM+, RIAM-COMPACT®, LES, RANS, Isolated hill*

1. Introduction

The lead author's research group has developed the numerical wind synopsis prediction technique named RIAM-COMPACT®. The core technology of RIAM-COMPACT® is under continuous development at the Research Institute for Applied Mechanics, Kyushu University. An exclusive license of the core technology has been granted by Kyushu TLO Co., Ltd. (Kyushu University TLO) to RIAM-COMPACT Co., Ltd. (http://www.riam-compact.com/), a venture corporation which was founded by the lead author and originated at Kyushu University in 2006. A trademark, RIAM-COMPACT®, and a utility model patent were granted to RIAM-COMPACT Co., Ltd. in the same year.

In the meantime, a software package has been developed based on the above-mentioned technique and is named the RIAM-COMPACT® natural terrain version software. Efforts have been made to promote this software as a standard model in the wind power industry. Some of the major corporations which have adopted the RIAM-COMPACT® software are Eurus Energy Holdings Corporation, Electric Power Development Co., Ltd. (J-POWER), Japan Wind Development Co., Ltd., EcoPower Co., Ltd., Mitsuuroko Green Energy Co., Ltd., West Japan Engineering Consultants, Inc., C-Tech Corporation, and Mitsubishi Heavy Industries, Ltd.

Computation time had been an issue of concern for the RIAM-COMPACT® software, which focuses on unsteady turbulence simulations (LES, Large-Eddy Simulation). The present fluid simulation solver is compatible with multi-core CPUs (Central Processing Units) such as the Intel Core i7 and also with GPGPU (General Purpose computing on GPU), which has drastically reduced the computation time, leaving no appreciable problems in terms of the practical use of the RIAM-COMPACT® software.

In the present study, simulation results of airflow over an isolated hill with steep slopes obtained from the RIAM-COMPACT® software are compared to those from another commercially available CFD (Computational Fluid Dynamics) software. The results from this comparison are reported.

2. Summary of Commercially Available CFD Software

Commercially available CFD software has developed mainly as an engineering tool primarily in the automobile and aviation industries until the present time. The following is a list of the major CFD software packages available on the market:

<u>General-purpose CFD thermal fluid analysis software</u>

■STAR-CCM+

http://www.cd-adapco.co.jp/products/star_ccm_plus/index.html

■ANSYS (CFD, Fluent, CFX)

http://ansys.jp/solutions/analysis/fluid/index.html

* Research Institute for Applied Mechanics, Kyushu University

** Tsubasa Windfarm Design

■SCRYU/Tetra
http://www.cradle.co.jp/products/scryutetra/

■STREAM
http://www.cradle.co.jp/products/stream/index.html

■CFD2000
http://www.cae-sc.jp/docs/cfd2000/index.htm

■PHOENICS
http://www.phoenics.co.jp/

■Autodesk Simulation CFD
http://www.cfdesign.com/

■CFD++
http://bakuhatsu.jp/software/cfd/

■CFD-ACE+
http://www.wavefront.co.jp/CAE/cfd-ace-plus/

■AcuSolve
http://acusolve.jsol.co.jp/index.html

■FLOW-3D
http://www.terrabyte.co.jp/FLOW-3D/flow3d.htm

■FloEFD
http://www.sbd.jp/product/netsu/floefd3cad.shtml

■Flow Designer
http://www.akl.co.jp/

■PowerFLOW
http://www.exajapan.jp/pages/products/pflow_main.html

■KeyFlow
http://www.kagiken.co.jp/product/keyflow/index.shtml

■OpenFOAM
http://www.cae-sc.jp/docs/FOAM/

■FrontFlow
http://www.advancesoft.jp/product/advance_frontflow_red/

The wind power industry has on its own developed and distributed CFD software designed for selecting sites appropriate for the installation of wind power generators (see the listing below). Recently, some of the above-mentioned general-purpose thermal fluid analysis software has started being adopted in the wind power industry.

CFD software designed for the wind power industry (wind farm design tools)

■RIAM-COMPACT®
http://www.riam-compact.com/

■MASCOT
http://aquanet21.ddo.jp/mascot/

■WindSim
http://www.windsim.com/

■METEODYN
http://meteodyn.com/

In the present study, the simulation results from the RIAM-COMPACT® software are compared to those from STAR-CCM+, one of the leading commercially available CFD software packages. The results of the comparison are discussed.

3. Summary of STAR-CCM+ Software

In this section, a summary of STAR-CCM+, a general-purpose thermal fluid analysis software package distributed by IDAJ Co., Ltd. (developer: CD-adapco) will be provided. The version of the software package used in the present study is 6.02.007 (for 64-bit Windows).

STAR-CCM+ uses a single GUI (Graphical User Interface) for computational mesh generation, execution of fluid analyses, and data post-processing. In the present study, a three-dimensional model of an isolated hill (IGES format) is created using CATIA, a three-dimensional CAD software package developed by Dassault Systèmes. After reading in the created three-dimensional CAD data on STAR-CCM+, the mesh type, the mesh spacing, the turbulence model (details to be described later), the time-step interval, the boundary conditions, and other variables are set. Subsequently, pre-processing, fluid analyses, and post-processing are performed.

The mesh generation method in STAR-CCM+ is distinctive. In STAR-CCM+, both a polyhedral mesh and a prism layer mesh can be used (see Fig. 1). The polyhedral mesh is a new type of mesh offered by CD-adapco and consists of polyhedral cells which possess 10 to 15 faces on average. The use of this cell type makes it possible to dramatically reduce the number of mesh cells required to obtain analysis results equivalent to those that can be obtained using a conventional tetrahedral mesh and 2) the memory required by the solver. With the use of this cell type, the computational stability improves significantly, and the time required to obtain convergent solutions also decreases. The prism layer mesh is a refined mesh designed to capture the behavior of the boundary layer developed over an object. In this type of mesh, layers of thin mesh cells are distributed regularly over the object. Since the thickness and the number

of layers in the normal direction with respect to the object surface can be freely adjusted, the behavior of the boundary layer in the vicinity of a wall can be captured with high accuracy. However, when the number of the prism layer mesh cells is very large, the computation time increases significantly.

Numerical simulations are based on FVM (Finite-Volume Method), and the Navier-Stokes equation is used as the governing equation. Iterative calculations are performed for the velocity and pressure fields using an AMG (Algebraic Multi-Grid) linear solver. For the time marching method, a first-order implicit method is used. For the convective term, a second-order upwind scheme is adopted for the case of RANS (Reynolds Averaged Navier-Stokes Simulation) models. For the case of LES models, a BCD (Bounded Central Differencing) scheme is employed.

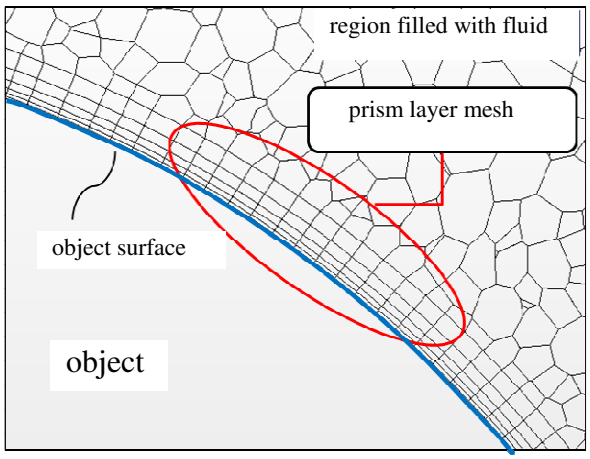

Fig. 1 Polyhedral mesh and prism layer mesh

4. Summary of RIAM-COMPACT®

In this section, a summary of the RIAM-COMPACT® natural terrain version software is provided. The RIAM-COMPACT® natural terrain version software uses collocated grids in a general curvilinear coordinate system in order to numerically predict local airflows over complex terrain with high accuracy while avoiding numerical instability. In these collocated grids, the velocity components and pressure are defined at the mesh cell centers, and variables which result from the contravariant velocity components multiplied by the Jacobian are defined at the cell faces. As for the simulation technique, the FDM (Finite-Difference Method) is adopted, and an LES model is used for the turbulence model. In LES, a spatial filter is applied to the flow field to separate eddies of various scales into GS (Grid Scale) components, which are larger than the computational grid cells, and SGS (Sub-Grid Scale) components, which are smaller than the computational grid cells. Large-scale eddies, i.e., the GS components of turbulence eddies, are directly numerically simulated without relying on the use of a physically simplified model. On the other hand, the main effect of small-scale eddies, i.e., the SGS components, is to dissipate energy, and this dissipation is modeled on the physical considerations of the SGS stress.

For the governing equations of the flow, a spatially-filtered continuity equation for incompressible fluid (Eq. (1)) and a spatially filtered Navier-Stokes equation (Eq. (2)) are used:

$$\frac{\partial \bar{u}_i}{\partial x_i} = 0 \qquad \text{-(1)}$$

$$\frac{\partial \bar{u}_i}{\partial t} + \bar{u}_j \frac{\partial \bar{u}_i}{\partial x_j} = -\frac{\partial \bar{p}}{\partial x_i} + \frac{1}{\mathrm{Re}} \frac{\partial^2 \bar{u}_i}{\partial x_j \partial x_j} - \frac{\partial \tau_{ij}}{\partial x_j} \qquad \text{-(2)}$$

Supporting equations are given in Eqs. (3) - (8):

$$\tau_{ij} \approx \overline{u_i' u_j'} \approx \frac{1}{3}\overline{u_k' u_k'}\delta_{ij} - 2\nu_{SGS}\bar{S}_{ij} \qquad \text{-(3)}$$

$$\nu_{SGS} = \left(C_s f_s \Delta\right)^2 \left|\bar{S}\right| \qquad \text{-(4)}$$

$$\left|\bar{S}\right| = \left(2\bar{S}_{ij}\bar{S}_{ij}\right)^{1/2} \qquad \text{-(5)}$$

$$\bar{S}_{ij} = \frac{1}{2}\left(\frac{\partial \bar{u}_i}{\partial x_j} + \frac{\partial \bar{u}_j}{\partial x_i}\right) \qquad \text{-(6)}$$

$$f_s = 1 - \exp\left(-z^+ / 25\right) \qquad \text{-(7)}$$

$$\Delta = \left(h_x h_y h_z\right)^{1/3} \qquad \text{-(8)}$$

Because mean wind speeds of 6 m/s or higher are considered in the present study, the effect of vertical thermal stratification (density stratification), which is generally present in the atmosphere, is neglected. Furthermore, the effect of surface roughness is included by reconstructing the irregularities of the terrain surface in high resolution.

The computational algorithm and the time marching method are based on a fractional-step (FS) method and the Euler explicit method, respectively. The Poisson's equation for pressure is solved by the SOR (Successive Over-Relaxation) method. For discretization of all the spatial terms in Eq. (2) except for the convective term, a second-order central difference scheme is applied. For the convective term, a third-order upwind difference scheme is applied. An interpolation technique based on four-point differencing and four-point interpolation by Kajishima[4] is used for the fourth-order central differencing that appears in the discretized form of the convective term. For the

weighting of the numerical diffusion term in the convective term discretized by third-order upwind differencing, $\alpha = 3$ is commonly applied in the Kawamura-Kuwahara Scheme[5]. However, $\alpha = 0.5$ is used in the present study to minimize the influence of numerical diffusion. For LES subgrid-scale modeling, the commonly used Smagorinsky model[6] is adopted. A wall-damping function is used with a model coefficient of 0.1.

5. Flow Field and Simulation Set-up

In this section, the flow field investigated and the coordinate system and simulation set-up adopted in the present study are described. The dimensions of the computational domain are 13h (x) × 9h (y) × 10h (z), where x, y, and z are the streamwise, spanwise, and vertical directions, respectively, and h is the height of the isolated hill (see Fig. 2). The geometry of the isolated hill is represented by the following function:

$$z(r)=0.5h\times\{1+\cos(\pi r/a)\},\ r=(x^2+y^2)^{1/2},\ a=2h \quad -(9)$$

where a is the radius of the isolated hill at its base.

Regarding the boundary conditions, uniform inflow conditions are applied at the inflow boundary, slip conditions are applied at the side and upper boundaries, and convective outflow conditions are applied at the outflow boundary. At the ground surface, non-slip boundary conditions are imposed. The Reynolds number is set to Re (=Uh/ν) = 10^4, where h is the isolated hill height and U is the wind speed at height h at the inflow boundary. The time steps are set to $\Delta t = 2 \times 10^{-3}(h/U)$ and $\Delta t = 1 \times 10^{-2}(h/U)$ in the simulations with RIAM-COMPACT® and STAR-CCM+, respectively.

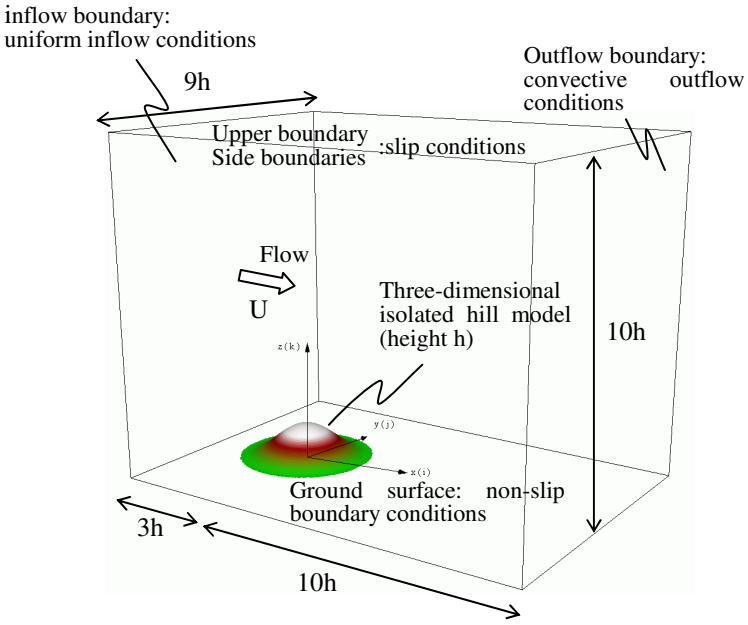

Fig. 2 Computational domain, coordinate system, and boundary conditions

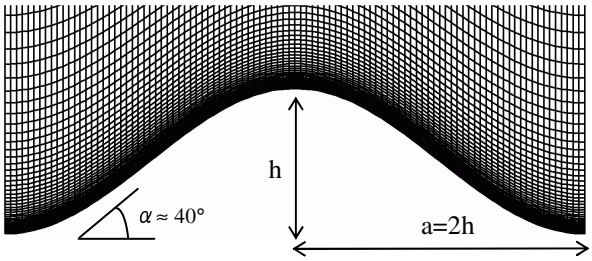

Fig. 3 Structured computational mesh used in the vicinity of the isolated hill in the RIAM-COMPACT simulation. The cross-section shown is for the central plane (y = 0).

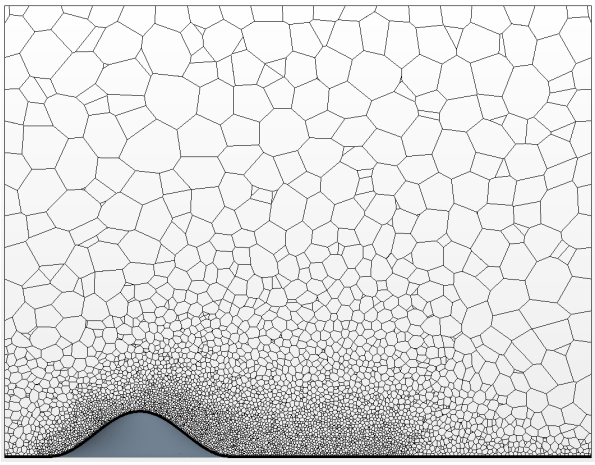

(a) Side view (y = 0)

(b) Top view (z = 0.5h)

Fig. 4 Side and top cross-sectional views of the computational mesh (unstructured mesh) distributed over the entire computational domain for the STAR-CCM+ simulations.

Fig. 3 shows the computational mesh (structured mesh) which is used in RIAM-COMPACT® in the vicinity of the isolated hill for the present simulation. The numbers of mesh points in the x-, y-, and z-directions are 326×226×67 points, respectively (approximately five million points in total). The mesh points in the x- and y-directions are spaced at an even interval of 0.04h while the mesh points in the z-direction are spaced unevenly (from 0.003h to 0.6h).

Fig. 4 shows the computational mesh (unstructured mesh) used in the present STAR-CCM+ simulations. The total number of mesh points is approximately one million (i.e., approximately 1/5 of that used in the RIAM-COMPACT® simulation). In the STAR-CCM+ simulations, the mesh resolution in the vicinity of the isolated hill is set to be nearly identical to that in the RIAM-COMPACT® simulation.

Tables 1 and 2 summarize all of the turbulence models (RANS, LES) adopted in the present comparative study. For convenience, simulations performed with the use of each of the models are referred to as Cases 1 to 5. In Case 4, i.e., the WALE model, the eddy viscosity coefficient becomes zero near the wall without the use of a wall damping function. Furthermore, this model has been designed in such a way that the eddy viscosity coefficient is not calculated for laminar shear layers.

RANS models	**Case 1**	Spalart-Allmaras single equation eddy-viscosity turbulence model, steady RANS
	Case 2	SST k-ω two-equation eddy -viscosity model, unsteady RANS (URANS)
LES models	**Case 3**	Smagorinsky model, LES
	Case 4	WALE model, LES

Table 1 Turbulence models used in the present STAR-CCM+ simulations

LES model	**Case 5**	Smagorinsky model, LES

Table 2 Turbulence model used in the present RIAM-COMPACT® simulation

6. Simulation Results and Discussions

First, the flow patterns which form in the vicinity of the isolated hill are examined (see Fig. 5). The qualitative behaviors of the flows numerically simulated by RIAM-COMPACT® and observed in a wind tunnel experiment resemble each other quite closely. More specifically, a shear layer separates in the vicinity of the top of the isolated hill and rolls up into isolated eddies, forming large eddies. Subsequently, these eddies are periodically shed downstream of the isolated hill. Refer to Uchida et al. for a detailed comparison between the simulation results from RIAM-COMPACT® and those from the wind tunnel experiment.

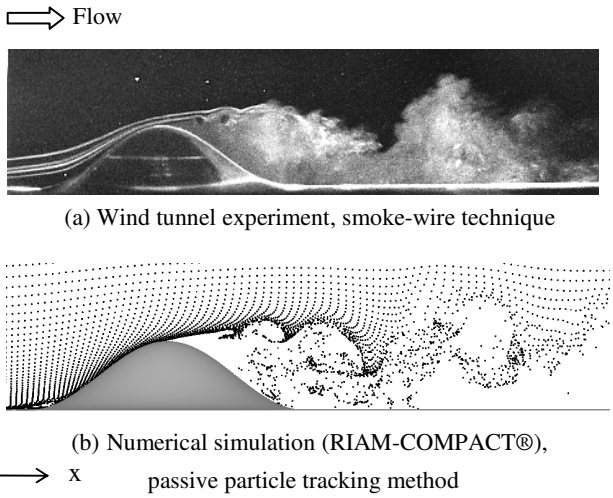

(a) Wind tunnel experiment, smoke-wire technique

(b) Numerical simulation (RIAM-COMPACT®), passive particle tracking method

Fig. 5 Visualization of the flow field in the vicinity of an isolated hill; instantaneous field

Figs. 6 to 12 illustrate comparisons of simulation results. In these figures, the time-averaged flow fields and turbulence statistics were evaluated from the fully developed flow field, specifically from the time interval of t = 100 - 200(h/U). Examinations of these figures (Figs. 6 to 10) reveal that the trends of the simulation results from STAR-CCM+ with the use of the RANS models (steady and unsteady) are similar to each other. In addition, the three sets of simulation results from STAR-CCM+ and RIAM-COMPACT® with the use of the LES models (i.e., STAR-CCM+ with the standard Smagorinsky model and the WALE model and RIAM-COMPACT® with the standard Smagorinsky model) resemble one another very closely with no distinction between the use of STAR-CCM+ and the use of RIAM-COMPACT®. It should be noted that a clear vortex center is simulated downstream of the isolated hill in the simulations with the LES models, however, not in the simulations with the RANS models.

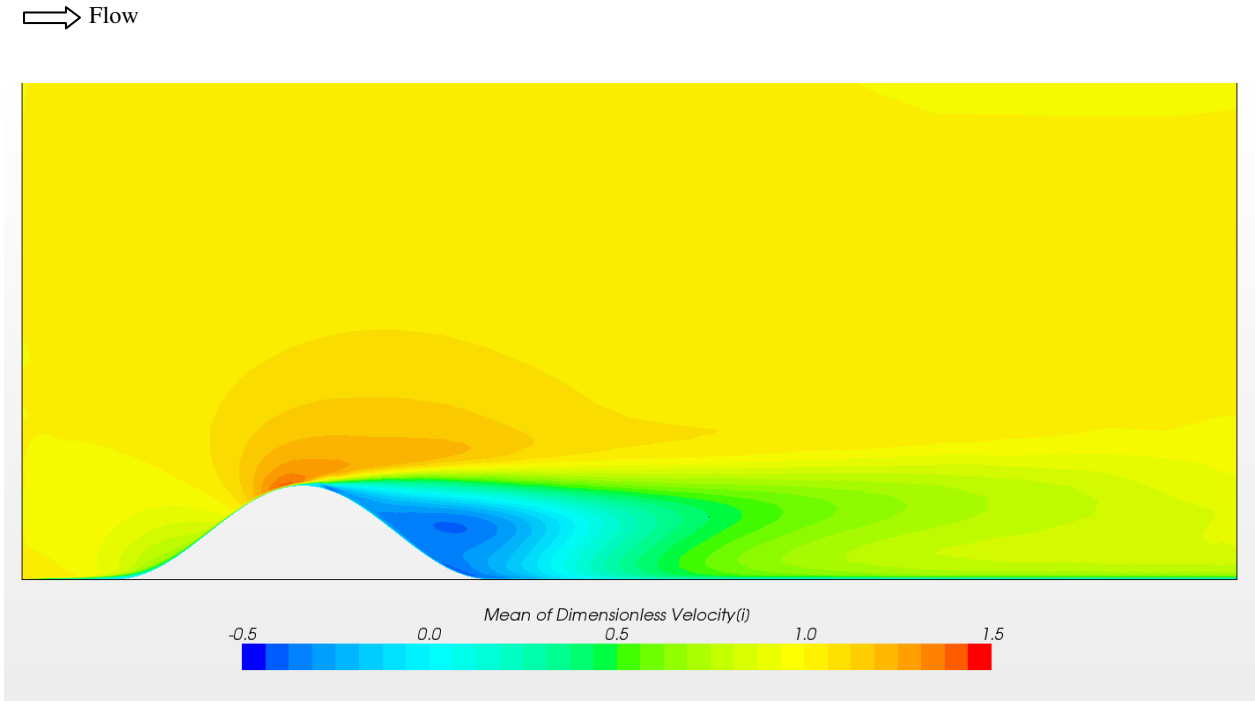

(a) Spalart-Allmaras single equation eddy-viscosity turbulence model, steady RANS

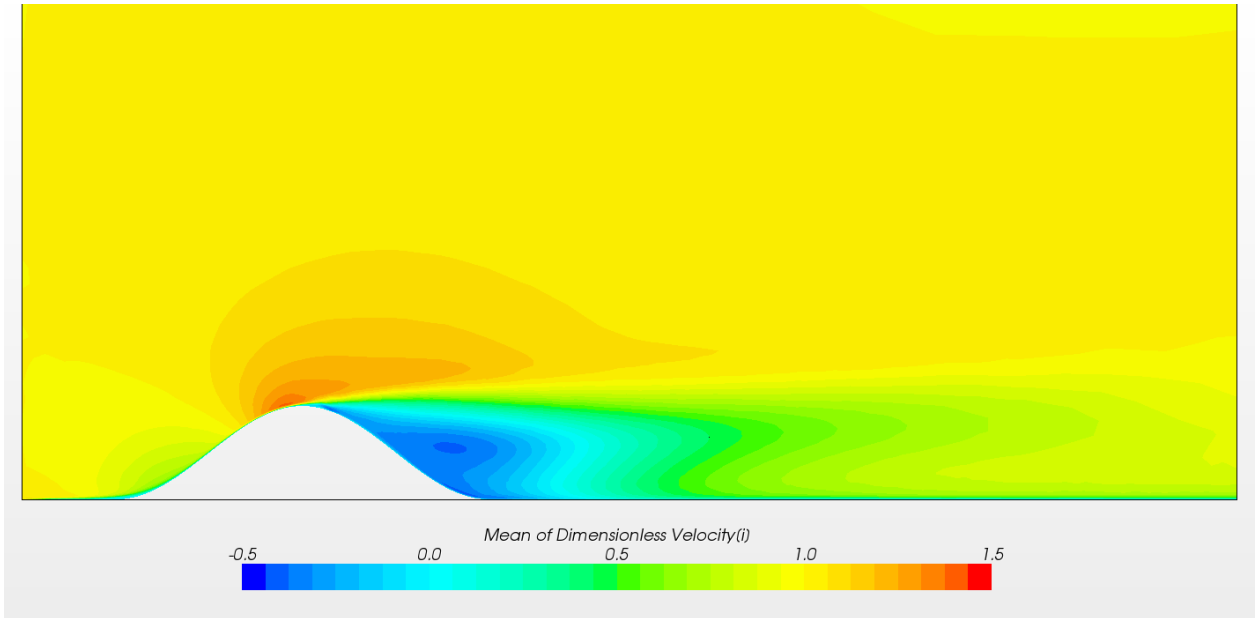

(b) SST k-ω two-equation eddy-viscosity model, unsteady RANS (URANS), time-averaged field

Fig. 6 Distribution of the streamwise (x) velocity component; simulation results from STAR-CCM+ with the use of RANS turbulence models. The cross-sections shown are for the central plane (y = 0) aligned with the streamwise direction (x).

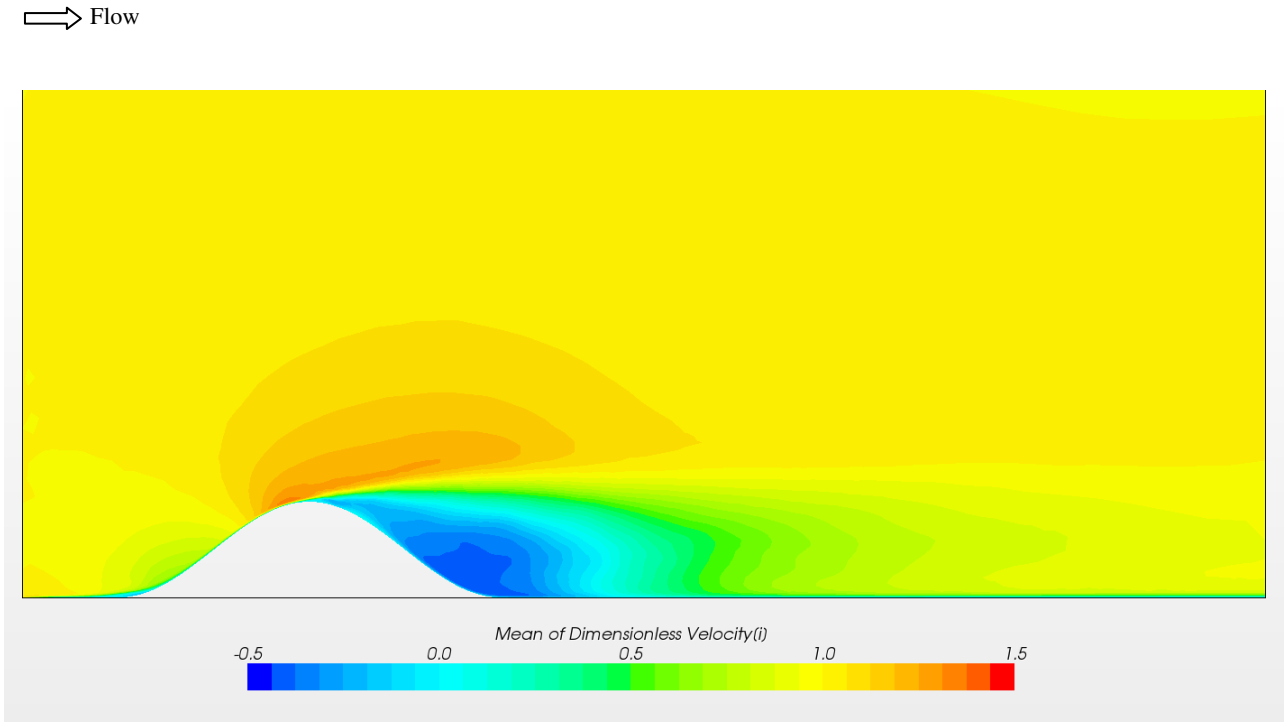

(a) The standard Smagorinsky model, LES

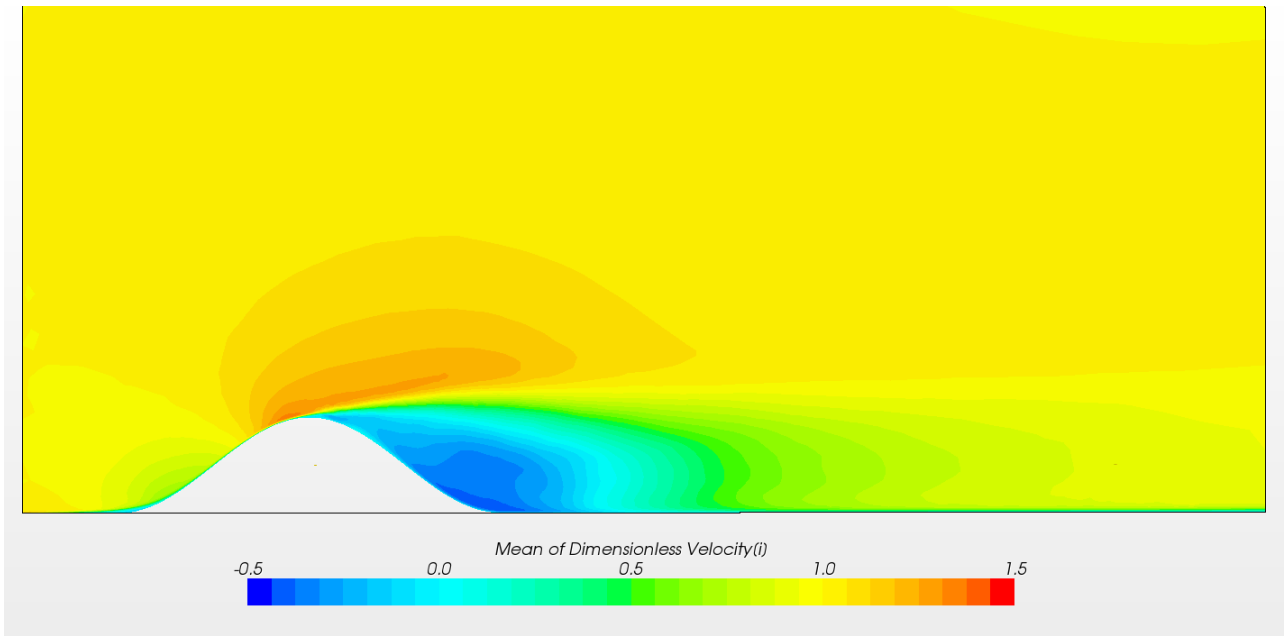

(b) The WALE model, LES

Fig. 7 Distribution of the time-averaged streamwise (x) velocity component; simulation results from STAR-CCM+ with the use of LES turbulence models. The cross-sections shown are for the central plane (y = 0) aligned with the streamwise direction (x).

⇨ Flow

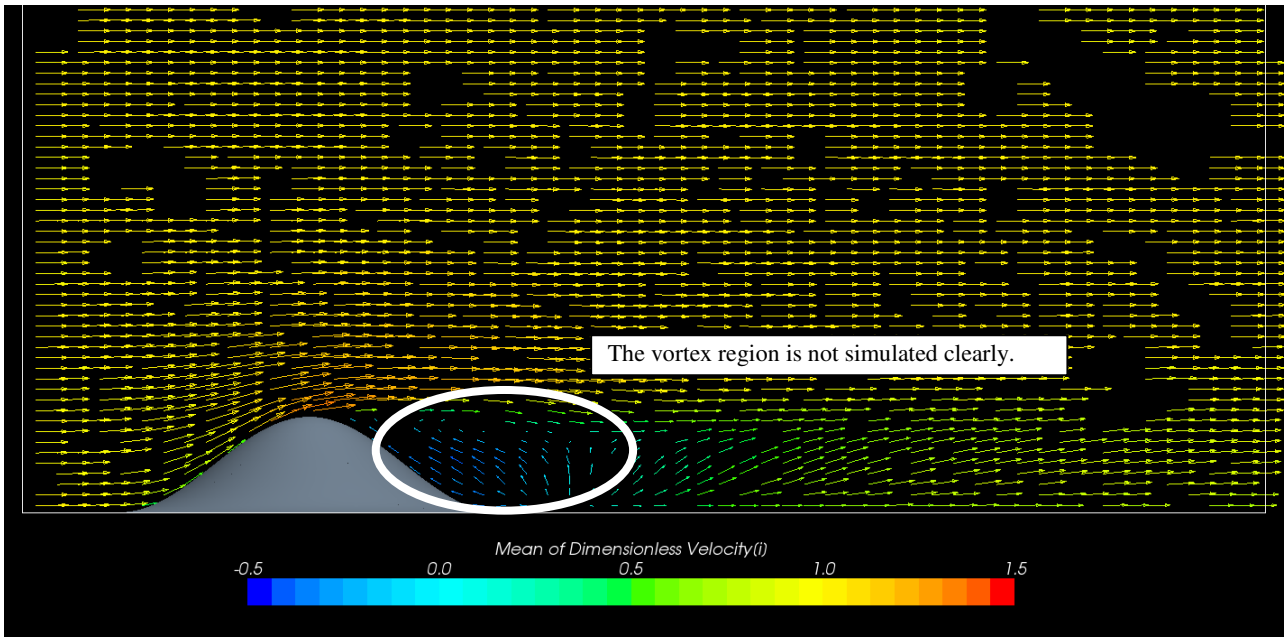

(a) Spalart-Allmaras single equation eddy-viscosity turbulence model, steady RANS

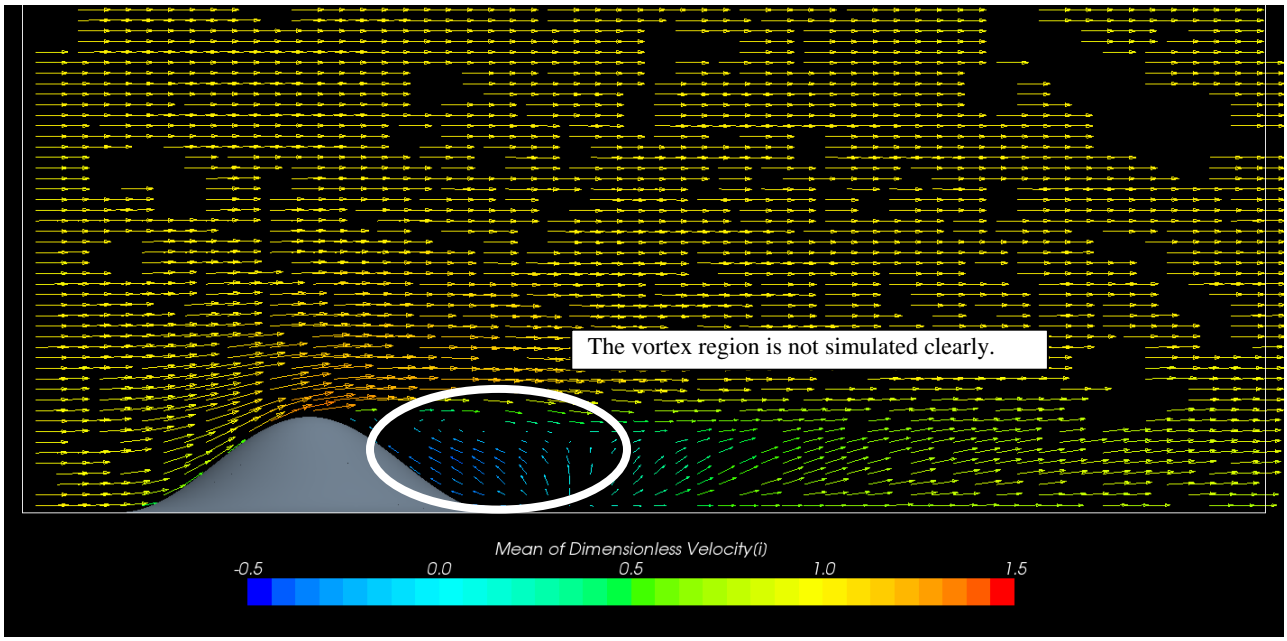

(b) SST k-ω two-equation eddy-viscosity model, unsteady RANS (URANS), time-averaged field

Fig. 8 Distribution of velocity vectors; simulation results from STAR-CCM+ with the use of RANS turbulence models. The cross-sections shown are for the central plane (y = 0) aligned with the streamwise direction (x).

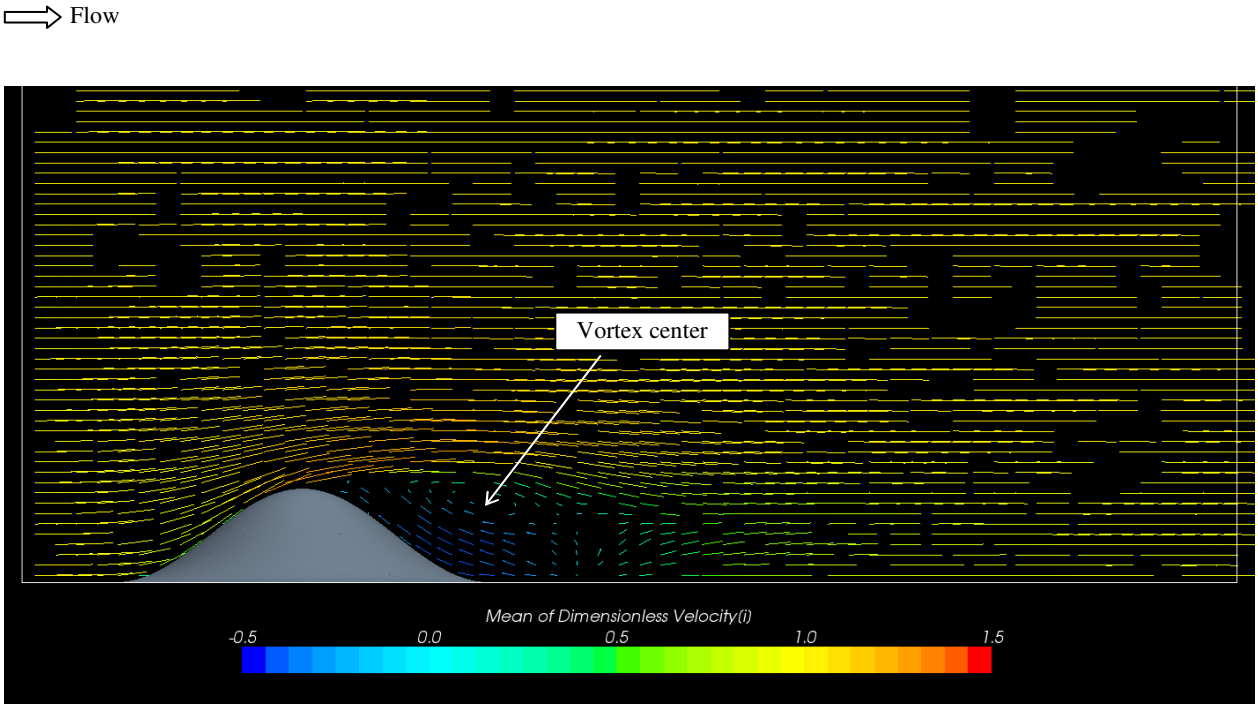

(a) The standard Smagorinsky model, LES

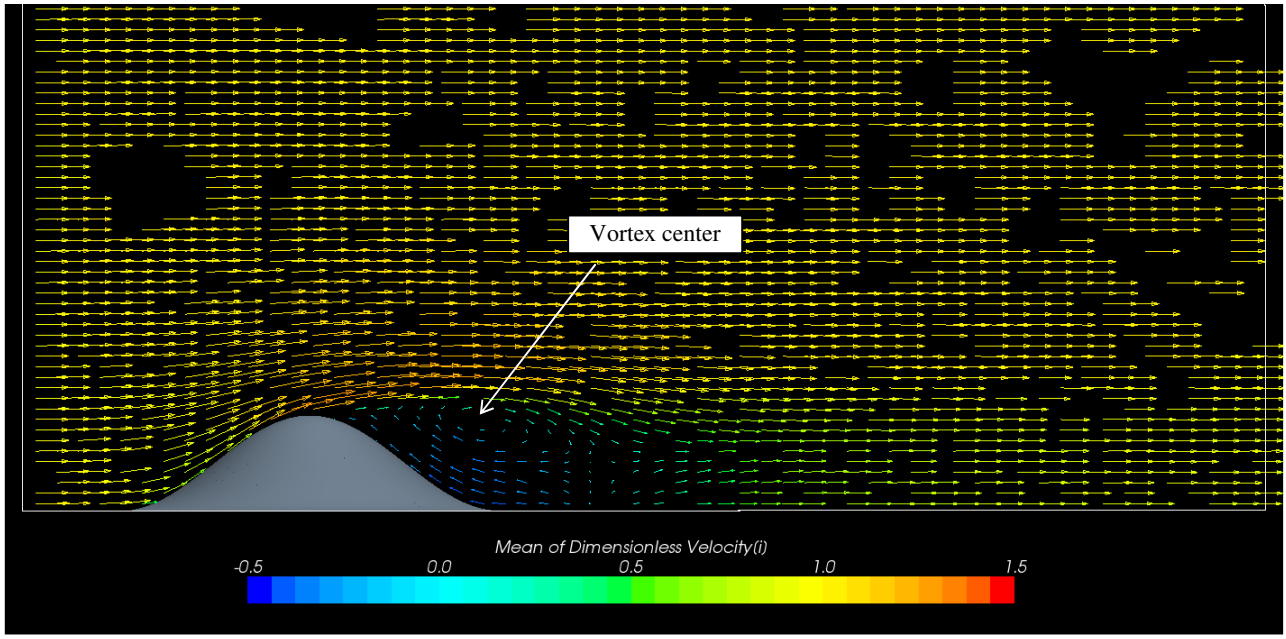

(b) The WALE model, LES

Fig. 9 Distribution of time-averaged velocity vectors; simulation results from STAR-CCM+ with the use of LES turbulence models. The cross-sections shown are for the central plane (y = 0) aligned with the streamwise direction (x).

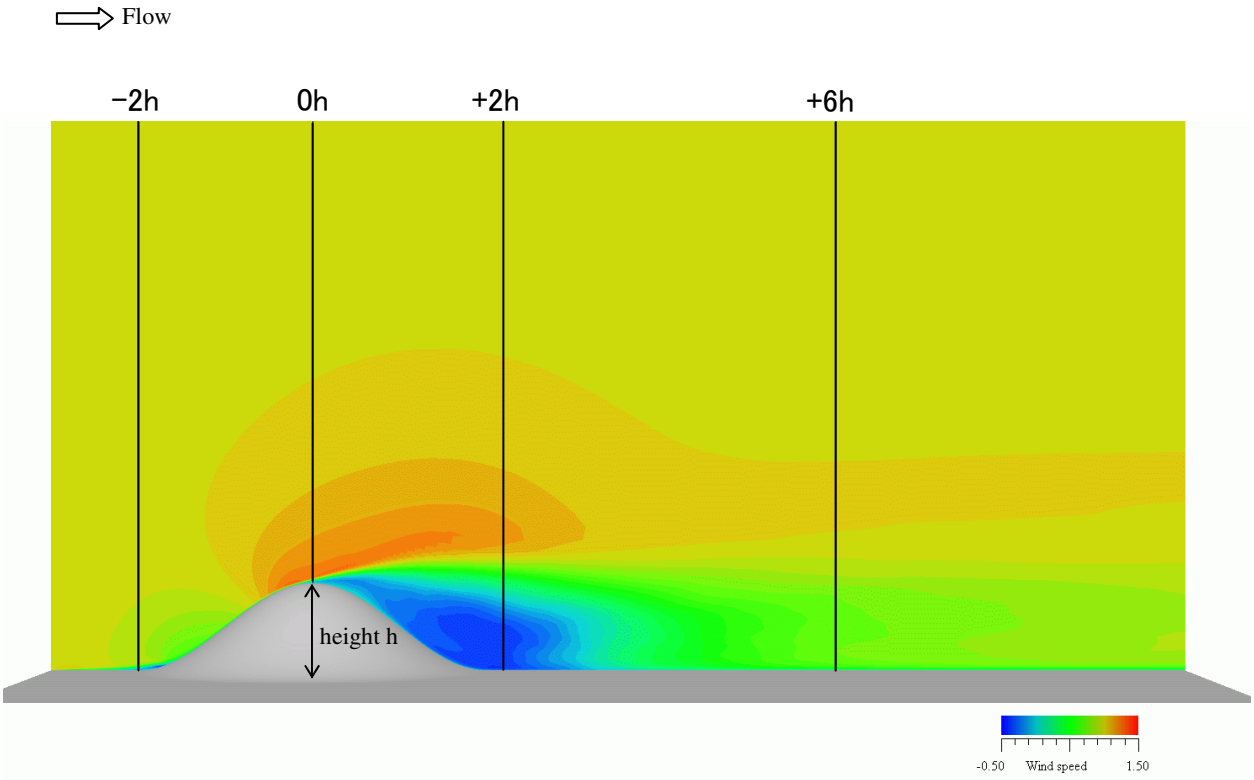

(a) Distribution of the streamwise (x) velocity component

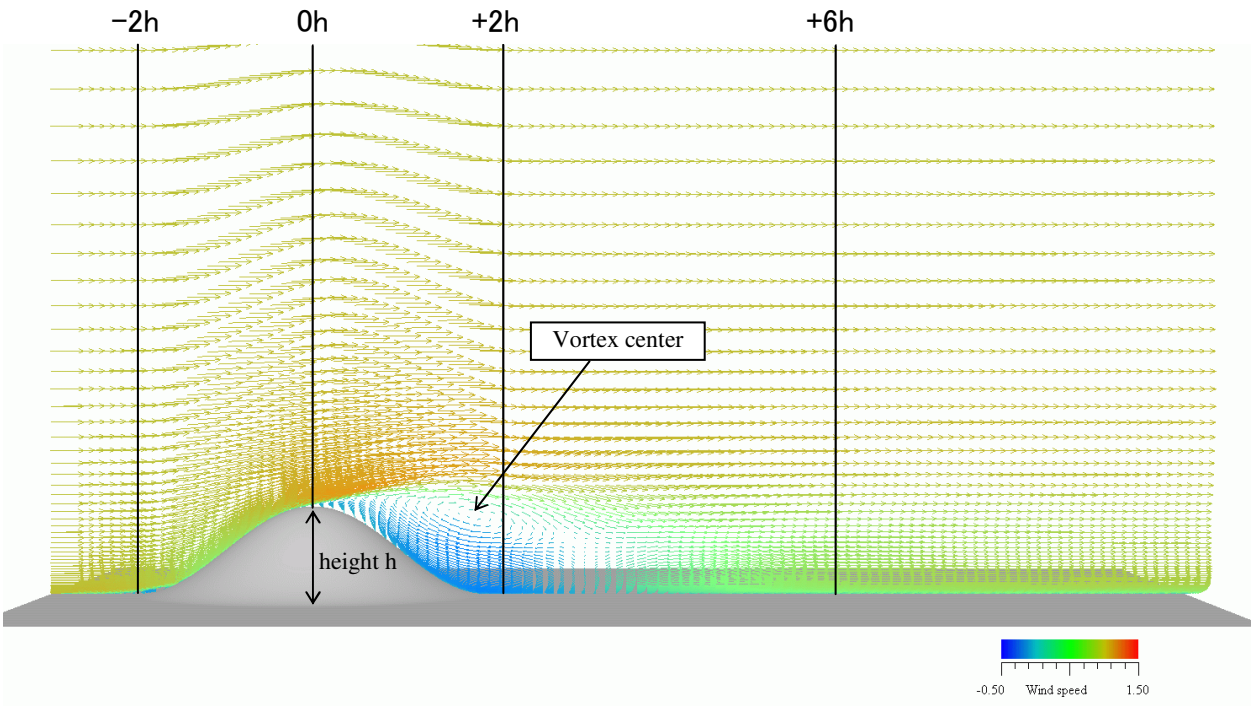

(b) Distribution of velocity vectors

Fig. 10 Time-averaged results from RIAM-COMPACT® with the use of the standard Smagorinsky LES model. The cross-sections shown are for the central plane (y = 0) aligned with the streamwise direction (x).

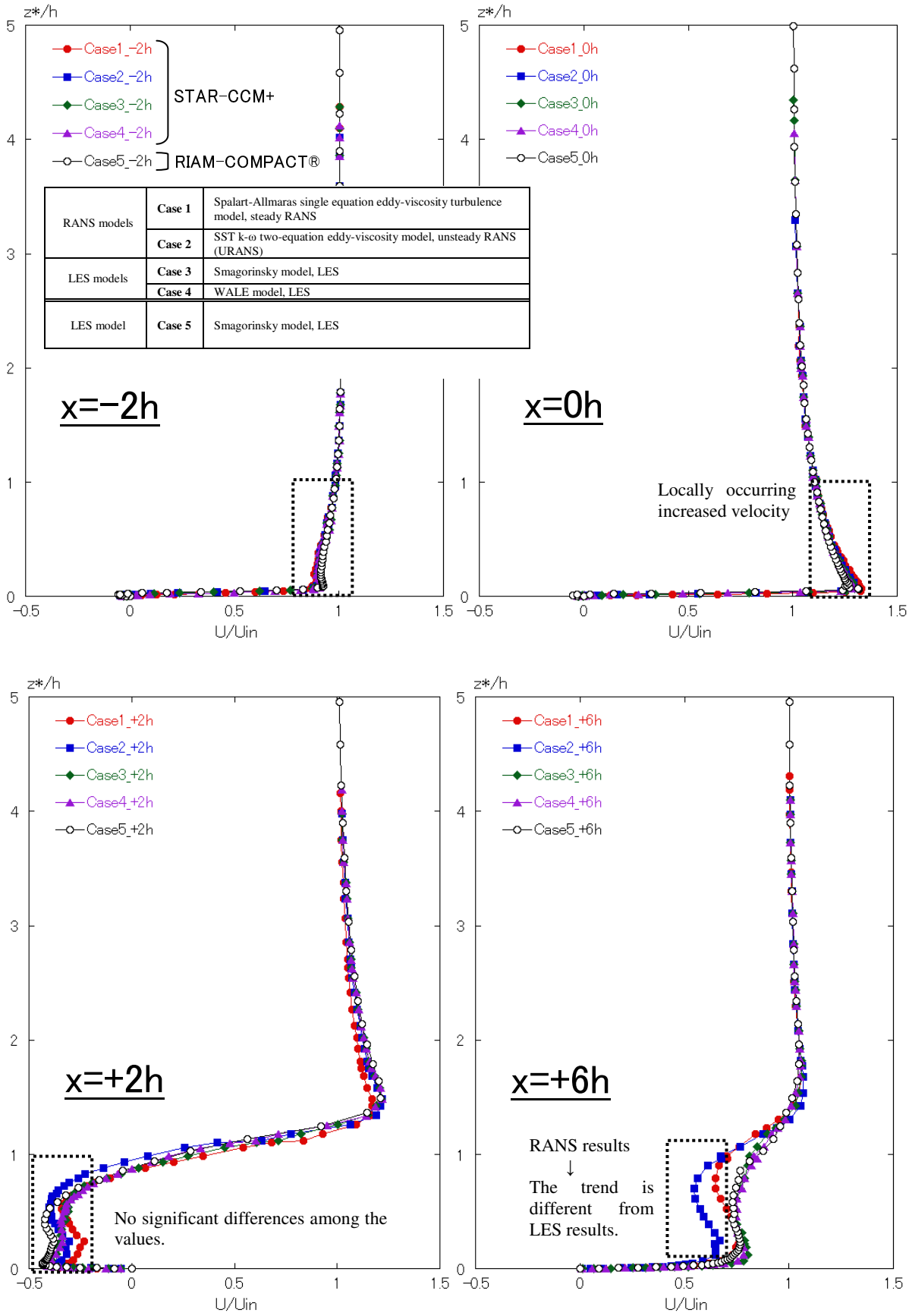

RANS models	**Case 1**	Spalart-Allmaras single equation eddy-viscosity turbulence model, steady RANS
	Case 2	SST k-ω two-equation eddy-viscosity model, unsteady RANS (URANS)
LES models	**Case 3**	Smagorinsky model, LES
	Case 4	WALE model, LES
LES model	**Case 5**	Smagorinsky model, LES

Fig. 11 Comparisons of profiles of the mean streamwise (x) velocity component

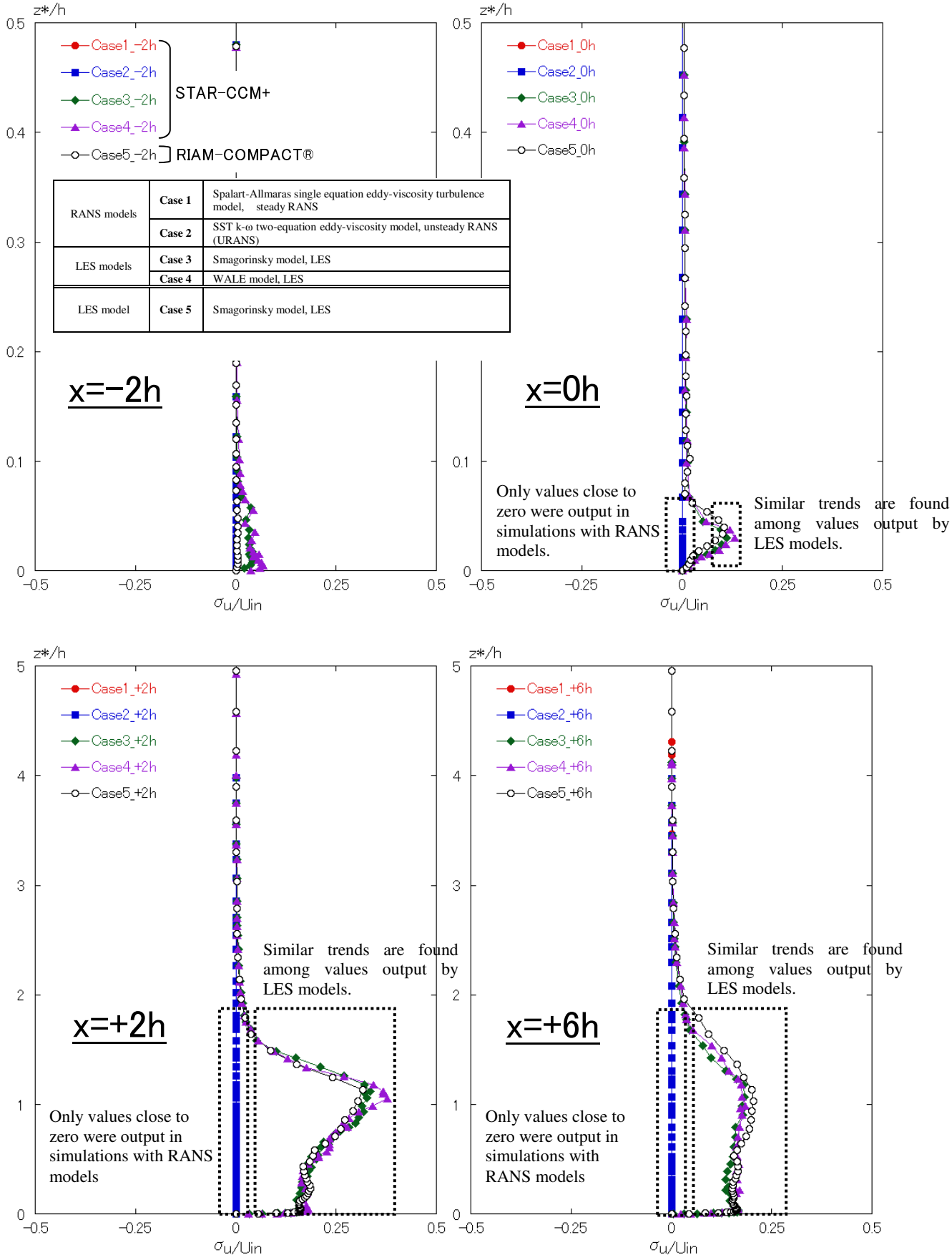

RANS models	**Case 1**	Spalart-Allmaras single equation eddy-viscosity turbulence model, steady RANS
	Case 2	SST k-ω two-equation eddy-viscosity model, unsteady RANS (URANS)
LES models	**Case 3**	Smagorinsky model, LES
	Case 4	WALE model, LES
LES model	**Case 5**	Smagorinsky model, LES

Fig. 12 Comparisons of profiles of the standard deviation of the streamwise (x) wind velocity component

Subsequently, the vertical profiles of turbulence statistics (the mean and standard deviation of the streamwise (x) velocity component), shown in Figs. 11 and 12, are examined. The turbulence statistics were evaluated at a total of four points, specifically, at x/h = -2, 0, +2, and +6 as shown in Fig. 10. In the mean velocity profiles, no significant differences are found at any of the points given by x/h = -2, 0, and +2 (Fig. 11). At the top of the isolated hill, which is located at x/h = 0, locally occurring increased wind velocity is evident. Immediately downstream of the isolated hill, that is at x/h = +2, a region of reversed flow is present. At x/h = +6, the trends of the wind velocity profiles differ between the simulation results from RANS models and those from LES models. From the point of view of predicting the airflow field over complex terrain, these errors in the simulation results from the RANS models would significantly affect assessments of the power to be generated and other variables. In the vertical profiles of the standard deviation of the streamwise (x) wind velocity component predicted by the RANS models, no significant differences are found at any of the four examined points (Fig. 12). Similarly, it can be said that the trends of the profiles from simulations which used the LES models, i.e., simulations by STAR-CCM+ with both the standard Smagorinsky model and the WALE model and the simulation by RIAM-COMPACT®, are nearly identical.

In the simulations performed in the present study, the number of mesh points used in RIAM-COMPACT® (structured mesh, approx. five million mesh points) is approximately five times that used in STAR-CCM+ (unstructured mesh, approx. one million mesh points). Nonetheless, it has been confirmed that the simulation by RIAM-COMPACT® completes approximately ten times faster than those by STAR-CCM+.

7. Conclusions

In the present paper, the airflow field in the vicinity of an isolated hill with steep slopes was simulated by one of the leading, commercially available CFD packages, STAR-CCM+ as well as by RIAM-COMPACT® (turbulence model: LES based on the Smagorinsky model). The simulation results were compared to examine the prediction accuracy of RIAM-COMPACT®. In STAR-CCM+, two types of RANS turbulence models were selected: the Spalart-Allmaras single equation eddy-viscosity turbulence model (steady RANS) and the SST k-ω two-equation eddy-viscosity model (unsteady RANS). In addition, for LES turbulence models (SGS models), the standard Smagorinsky model and the WALE model were selected.

From the comparisons of the simulation results, the following have been found. Images visualizing the flow fields time-averaged over the interval of t = 100 - 200(h/U) suggested that the trends of the simulation results from STAR-CCM+ with the RANS turbulence models (steady and unsteady) were quite similar to each other. In addition, the trends of the flow patterns simulated by RIAM-COMPACT® with the LES turbulence model (the standard Smagorinsky model) and STAR-CCM+ with the LES turbulence models (the standard Smagorinsky model and the WALE model) were nearly the same. In addition, the center of the vortex (region of reversed flow) downstream of the isolated hill which was evident in the LES simulations, was not adequately simulated by STAR-CCM+ using the RANS turbulence models.

In the present study, the vertical profiles of turbulence statistics (the mean and standard deviation of the streamwise (x) wind velocity component) were evaluated and compared at four points, x/h = -2, 0, +2, and +6. The comparisons revealed the following. No significant difference was found among the mean velocity profiles obtained from all the turbulence models at x/h = -2, 0, and +2. At the top of the isolated hill, which was located at x/h = 0, locally occurring increased velocity was identified. At x/h = +2, which was immediately downstream of the isolated hill, an area of negative velocity was found, indicating the presence of a region of reversed flow. At x/h = +6, the trends of the results differed between the simulations which used the RANS models and those which used the LES models. From the perspective of predicting the airflow field over complex terrain, the prediction errors in the mean wind velocity in the RANS model simulations would greatly affect the assessments of the power to be generated and other variables. In the simulations which used the RANS turbulence models, the values of the standard deviation were not significantly different from zero throughout the profiles at all the examined points. In the simulations which used the LES models, i.e., STAR-CCM+ with the standard Smagorinsky model and the WALE model and RIAM-COMPACT® with the standard Smagorinsky model, the trends of the profiles of the mean and standard deviation of the wind velocity resembled one another quite closely as was the case for the trends of the visualized flow field.